Volume 4 | Number 7 | July 2014 | Pages 1839–2162

Catalysis Science & Technology

www.rsc.org/catalysis

ISSN 2044-4753

ROYAL SOCIETY OF CHEMISTRY

PAPER
Zhong-Ning Xu, Guo-Cong Guo *et al.*
MgO: an excellent catalyst support for CO oxidative coupling to dimethyl oxalate

Catalysis Science & Technology

PAPER

View Article Online
View Journal | View Issue

MgO: an excellent catalyst support for CO oxidative coupling to dimethyl oxalate

Cite this: *Catal. Sci. Technol.*, 2014, 4, 1925

Si-Yan Peng,[ab] Zhong-Ning Xu,*[a] Qing-Song Chen,[a] Zhi-Qiao Wang,[a] Yumin Chen,[a] Dong-Mei Lv,[a] Gang Lu[a] and Guo-Cong Guo*[a]

Received 25th February 2014,
Accepted 16th April 2014

DOI: 10.1039/c4cy00245h

www.rsc.org/catalysis

Pd/MgO catalysts are found, for the first time, to be extraordinarily active and stable for CO oxidative coupling to dimethyl oxalate. A series of Pd/MgO catalysts with Pd loadings of 0.1, 0.3, 0.5, 1 and 2 wt% were prepared by a wet impregnation method and systematically characterized by XRD, TEM, ICP, UV-DRS, H_2-TPR and CO_2-TPD. It has been demonstrated that the amount of Pd loading has a pronounced effect on the catalytic activity for CO oxidative coupling to dimethyl oxalate. CO conversion increases with the increase of the Pd loading due to high dispersion and similar sizes of Pd nanoparticles, as well as, the increase in number of surface active sites.

1. Introduction

Dimethyl oxalate (DMO) is an important chemical raw material and intermediate for the syntheses of oxalic acid, oxamide, dyes, pharmaceuticals, *etc.*[1] More importantly, hydrogenation of DMO can also be used to synthesize ethylene glycol (EG),[2–5] which is a considerable chemical feedstock with a global demand of about 25 million tons each year. Commercial EG is mainly produced from ethylene oxide hydrolysis.[6] Considering the soaring price of crude oil and the depletion of petroleum resources, a new EG synthesis technology called coal to ethylene glycol (CTEG) developed by our institute is attracting growing interest because of its green and atom economy.[7,8] CTEG includes three main processes: 1) elimination of a small amount of hydrogen gas in CO separated from coal-derived synthesis gas; 2) CO oxidative coupling to DMO: $2CH_3ONO + 2CO \rightarrow (COOCH_3)_2 + 2NO$; and 3) hydrogenation of DMO to EG. Among these, CO oxidative coupling to DMO is the crucial step to realize the conversion of inorganic C1 to organic C2 in CTEG.[9]

Pd/α-Al_2O_3 has been widely considered as an active catalyst for CO oxidative coupling to DMO.[10–14] However, there are still several problems to be solved despite considerable efforts that have been dedicated to the study of the CO oxidative coupling process. To date, the Pd loading of an industrial catalyst for CO oxidative coupling to DMO is relatively high at 2 wt% (the state of the art), resulting in a greatly increased cost of production. Moreover, the catalytic mechanism of CO oxidative coupling to DMO remains controversial. Pd based catalysts supported on other supports with high activity for CO oxidative coupling to DMO are rather limited. Pd catalysts with different supports for CO oxidative coupling to DMO have been summarized by Uchiumi *et al.*, and the results have demonstrated that Pd catalysts supported on NaY zeolites, silica, activated alumina, and activated carbon show much lower activities compared to Pd/α-Al_2O_3.[15] Zhao *et al.*[1] reported a high efficiency Pd based catalyst supported on carbon nanofibers for the synthesis of DMO, but the Pd loading of the catalyst was still high (1 wt%). It is well established that the support effect has a significant influence on many heterogeneous catalytic reactions, such as CO oxidation,[16,17] methane combustion,[18] hydrogenation of nitrobenzene,[19] ethylene oxidation,[20] and acrylonitrile decomposition.[21] Acid–base and redox properties of the support and metal–support interactions can greatly affect the catalytic performance of supported catalysts. Therefore, designing efficient Pd based nanocatalysts by making use of the support effect is necessary and important from the points of view of both fundamental study and industry application.

It is desirable and practical to develop high performance Pd based catalysts supported on other supports for CO oxidative coupling to DMO. In this work, we firstly discovered an excellent MgO support and further developed a low Pd loading (*ca.* 0.5 wt%) Pd/MgO catalyst with high activity, selectivity and stability for CO oxidative coupling to DMO.

2. Experimental

2.1. Catalyst preparation

A series of Pd/MgO catalysts with 0.1, 0.3, 0.5, 1 and 2% (by weight) Pd loadings were prepared by a wet impregnation method and by controlling the amount of the palladium acetate precursor. The MgO support was impregnated with an

[a] *State Key Laboratory of Structural Chemistry, Fujian Institute of Research on the Structure of Matter, Chinese Academy of Sciences, Fuzhou, Fujian 350002, PR China. E-mail: gcguo@fjirsm.ac.cn; Fax: +86 591 83714946; Tel: +86 591 83512502*

[b] *Key Laboratory of Coal to Ethylene Glycol and Its Related Technology, Chinese Academy of Sciences, Fuzhou, Fujian 350002, PR China*

acetone solution of palladium acetate under vigorous magnetic stirring and then the mixed solution was heated at 50 °C until the acetone was evaporated completely. The sample was calcined at 400 °C for 4 h to form PdO/MgO. Prior to the activity evaluation, the calcined sample was reduced in a hydrogen atmosphere to obtain Pd/MgO. The calcined samples were denoted as 0.1%-PdO/MgO, 0.3%-PdO/MgO, 0.5%-PdO/MgO, 1%-PdO/MgO and 2%-PdO/MgO, and the reduced catalysts were thus denoted as 0.1%-Pd/MgO, 0.3%-Pd/MgO, 0.5%-Pd/MgO, 1%-Pd/MgO and 2%-Pd/MgO.

Other supported Pd catalysts such as Pd/α-Al_2O_3, Pd/TiO_2, Pd/γ-Al_2O_3 and Pd/AC (activated charcoal) were prepared by the same method for comparison. The theoretical Pd loadings of these catalysts were 0.5 wt%, and the actual Pd loadings were measured by Inductively Coupled Plasma (ICP) spectroscopy.

2.2. Catalyst characterization

Powder X-ray diffraction (XRD) patterns were measured on a glass wafer using a Rigaku MiniFlex II diffractometer with a Cu-Kα X-ray source (λ = 1.5406 Å) at a scan speed of 5° min^{-1} (2θ). The X-ray tube was operated at 40 kV and 30 mA. Samples for transmission electron microscopy (TEM) observations were prepared by drying a drop of diluted ethanol dispersion of Pd/MgO catalysts on copper grids. Images were obtained by TEM (Tecnai G2 F20) carried out at 200 kV. ICP elemental analysis measurements were carried out using an Ultima 2 plasma emission spectrometer from Jobin Yvon. UV-visible diffuse reflectance spectra (UV-DRS) were measured using a PE Lambda 950 spectrophotometer equipped with a diffuse reflectance accessory and were recorded in the range of 400–850 nm using $BaSO_4$ as the reference sample. Temperature programmed reduction (TPR) and temperature programmed desorption (TPD) of CO_2 experiments were carried out using an Altamira AMI-300 instrument equipped with a thermal conductivity detector (TCD). Prior to conducting the H_2-TPR experiment, 100 mg of sample placed in a quartz U-tube was first heated to 400 °C for 1 h under a flow of argon (30 mL min^{-1}). After cooling to room temperature, the sample was exposed to 10% H_2–Ar mixture (30 mL min^{-1}) and then heated to 500 °C at a rate of 10 °C min^{-1}. The basic properties of the catalysts were examined by the CO_2-TPD technique. In a typical experiment, 100 mg of sample was treated with helium at 400 °C for 2 h to remove the adsorbed impurities. After cooling to 25 °C under a helium flow, the sample was exposed to 40% CO_2–He mixture (50 mL min^{-1}) for 1 h, followed by purging with helium for 30 min, and then heated to 800 °C by ramping at 10 °C min^{-1} under flowing helium.

2.3. Activity evaluation

The activity of the catalysts for CO oxidative coupling to DMO was evaluated in a fixed-bed quartz tubular reactor. The catalysts (200 mg) were placed in the center of the quartz tubular reactor. The reactant gases (28% CO, 20% CH_3ONO, 4% Ar and N_2 balance) were passed through the reactor at a gas hourly space velocity (GHSV) of 3000 h^{-1}. The catalytic activity tests were performed under atmospheric pressure. The composition of the reactant gases and reaction products was monitored using an on-line Shimadzu GC-2014 gas chromatograph equipped with a thermal conductivity detector and a flame ionization detector.

The conversion of CO, the selectivity to DMO and the space-time yields (STY) of DMO were calculated using the following formulas:

$$\text{Conversion of CO (\%)} = (1 - ([\text{Ar}]_{in}/[\text{Ar}]_{out})/([\text{CO}]_{in}/[\text{CO}]_{out})) \times 100\%$$

$$\text{Selectivity to DMO (\%)} = (S_{DMO} \times \text{R-F}_{DMO})/(S_{DMO} \times \text{R-F}_{DMO} + S_{DMC} \times \text{R-F}_{DMC}) \times 100\%$$

$$\text{STY of DMO (g L}^{-1}\text{ h}^{-1}\text{)} = \text{conversion of CO} \times \text{selectivity to DMO} \times \text{GHSV of CO} \times 118.09\text{ g mol}^{-1}/(2 \times 22.4\text{ L mol}^{-1})$$

where $[Ar]_{in}$ and $[Ar]_{out}$ are the concentrations of Ar at the inlet and outlet, $[CO]_{in}$ and $[CO]_{out}$ are the concentrations of CO at the inlet and outlet, respectively, S_{DMO} and S_{DMC} are the peak areas of dimethyl oxalate and dimethyl carbonate and R-F_{DMO} and R-F_{DMC} are the relative correction factors of dimethyl oxalate and dimethyl carbonate, respectively.

3. Results and discussion

3.1 Catalytic activity

The evaluation of the catalytic performance for CO oxidative coupling to DMO was carried out using a home-made catalytic evaluation device. Table 1 summarizes the catalytic performance for CO oxidative coupling to DMO over Pd/MgO,

Table 1 CO oxidative coupling to DMO on different catalysts[a]

Catalysts	Actual Pd loading (%)	Conversion[b] (%)	Selectivity[c] (%)	STY[d] (g L^{-1} h^{-1})
Pd/MgO	0.42	63	97	1353
Pd/α-Al_2O_3	0.46	56	94	1166
Pd/TiO_2	0.43	26	90	518
Pd/γ-Al_2O_3	0.41	20	88	390
Pd/AC	0.42	15	89	296

[a] Reaction conditions: 200 mg of the catalyst, theoretical Pd loading of 0.5 wt%, gas hourly space velocity (GHSV) of 3000 h^{-1}, reactants CO/CH_3ONO volume ratio: 1.4, 0.1 MPa, 130 °C. [b] Conversion of CO. [c] Selectivity to DMO. [d] STY represents the space-time yield in grams of DMO per liter of the catalyst per hour (g L^{-1} h^{-1}).

Pd/α-Al_2O_3, Pd/TiO_2, Pd/γ-Al_2O_3 and Pd/AC catalysts, which were prepared by the same method and evaluated under the same reaction conditions. It is interesting to find that Pd/MgO exhibits remarkable catalytic performance for CO oxidative coupling to DMO, even exceeding that of Pd/α-Al_2O_3, whereas other supported catalysts show much lower activities for this reaction. The CO oxidative coupling activity is in the order of Pd/MgO > Pd/α-Al_2O_3 > Pd/TiO_2 > Pd/γ-Al_2O_3 > Pd/AC, which demonstrates that the catalytic activity for CO oxidative coupling to DMO is strongly dependent on the nature of the support materials.

Fig. 1 shows CO conversion over Pd/MgO catalysts with different Pd loadings as a function of reaction temperature. The temperature dependence of CO conversion indicates that the activity of Pd/MgO catalysts for CO oxidative coupling to DMO increases gradually as the temperature is increased from 90 to 150 °C. Moreover, the amount of Pd loading also has a significant influence on the catalytic activity for CO oxidative coupling to DMO. By and large, CO conversion increases with the increase of Pd loading, but not in proportion to it. However, the high Pd loading will result in a greatly increased cost of catalysts due to the expensive price and extreme shortage of the Pd noble metal. The 0.5%-Pd/MgO catalyst exhibits high activity and selectivity with 63% CO conversion and 97% selectivity to DMO under the same reaction conditions as those for the industrial catalyst. Moreover, CO conversion can reach up to 68.7% at 150 °C, close to the theoretical maximum value of 71.4%. Therefore, a Pd loading of around 0.5 wt% is identified as the optimum content from both catalytic performance and economical points of view. The stability investigation of the 0.5%-Pd/MgO catalyst was carried out with a duration lifetime test for 120 h at 130 °C. As shown in Fig. 2, the excellent catalytic performance can be stable over 120 h, which lays a good foundation for further extending the long-term stability. Furthermore, Pd/MgO was prepared *via* a wet impregnation method, which is flexible in controlling the Pd loading and suitable for its large-scale production.

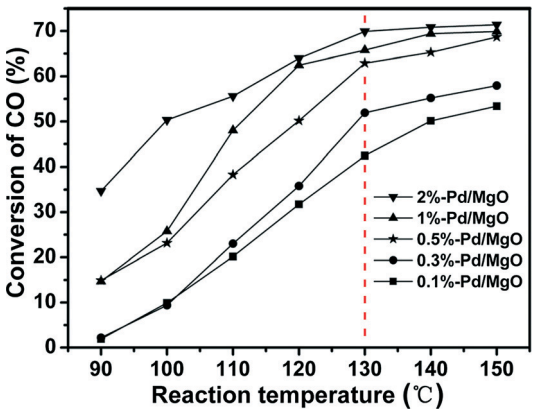

Fig. 1 Conversion of CO over Pd/MgO catalysts with different Pd loadings for CO oxidative coupling to DMO at different reaction temperatures.

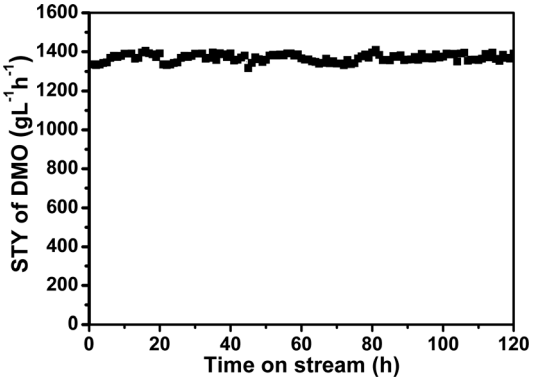

Fig. 2 Space-time yield of DMO over a 0.5%-Pd/MgO catalyst (200 mg) at 130 °C for 120 h.

3.2 Catalyst characterization

Fig. 3 presents the TEM images and the size distribution histograms of Pd/MgO catalysts. Obviously, the Pd nanoparticles of all catalysts are highly dispersed on the surface of the MgO support, suggesting that the Pd nanoparticles did not aggregate with the increase of the Pd loading. The number of Pd nanoparticles increased significantly with the increase of the Pd loading, but the average size of the Pd nanoparticles remained nearly unchanged. The average sizes of the Pd nanoparticles over all catalysts are in the range of 4.1–4.5 nm. It should be mentioned that the size statistics of the 0.1%-Pd/MgO catalyst cannot be obtained since few Pd nanoparticles can be observed (Fig. 3a). However, the size of the existing Pd nanoparticles over the 0.1%-Pd/MgO catalyst is similar to those of other catalysts. In addition, the size distributions of Pd nanoparticles over all catalysts are very narrow and uniform and show no marked differences. Therefore, the number of active sites will increase as the Pd loading increases from 0.1 to 2 wt%, which contributes mainly to the increasing catalytic activity for CO oxidative coupling to DMO (Fig. 1). It should be noted that the morphology and the size distribution of Pd nanoparticles of 0.5%-Pd/MgO after the durability test for 120 h (Fig. 3f) are very similar to those of the fresh catalyst (Fig. 3c). This implies that neither aggregation nor sintering of the Pd nanoparticles of 0.5%-Pd/MgO occurred during the lifetime evaluation process, which illustrates the high stability of the 0.5%-Pd/MgO catalyst.

Fig. 4 shows the XRD patterns of Pd/MgO catalysts with different Pd loadings. The sharp diffraction peaks are observed for all of the five catalysts at 2θ = 37.1, 43.1, 62.4, 74.8, and 78.6°, which are assigned to the crystalline phase of the MgO support.[22] No Pd diffraction peaks are observed for the 0.1%-Pd/MgO, 0.3%-Pd/MgO, 0.5%-Pd/MgO and 1%-Pd/MgO catalysts, indicating that the Pd nanoparticles are highly dispersed on the surface of MgO or that the amounts of Pd loading are too small to be detected. When the Pd loading is raised to 2 wt%, there is a new weak diffraction peak at 40° observed for the 2%-Pd/MgO catalyst, corresponding to the face-centered cubic (fcc) Pd (111) characteristic diffraction.

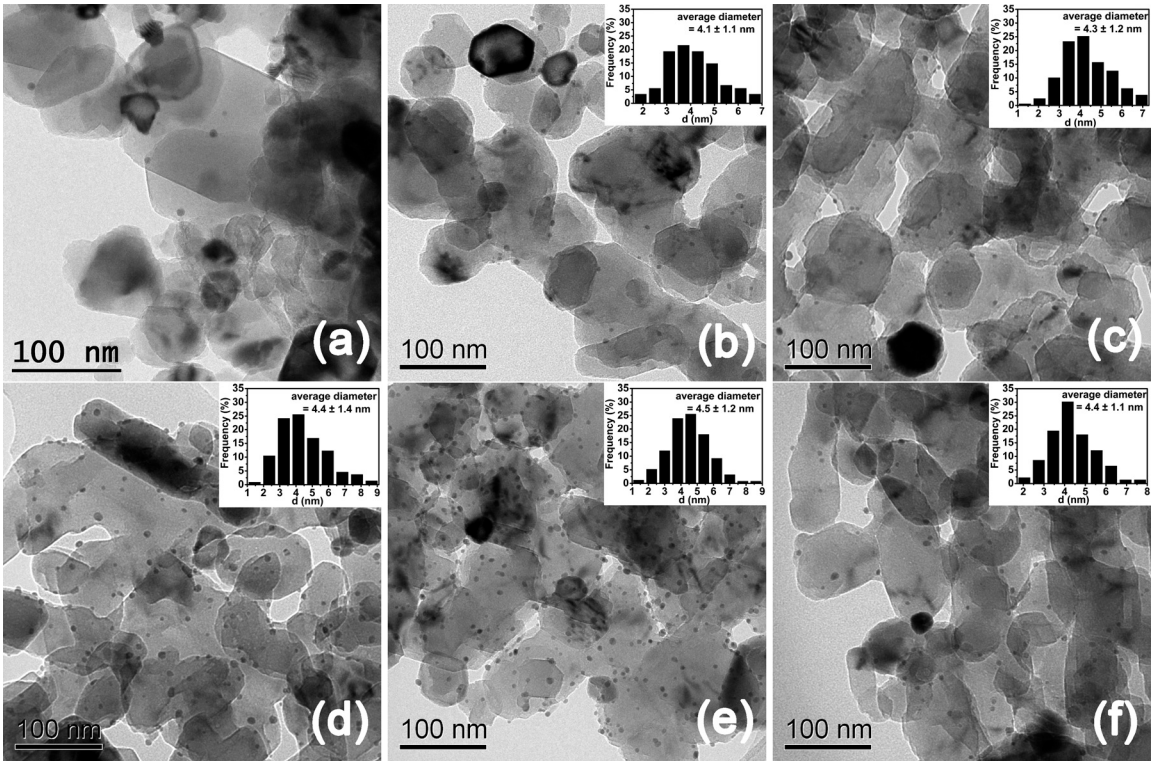

Fig. 3 TEM images of 0.1%-Pd/MgO (a), 0.3%-Pd/MgO (b), 0.5%-Pd/MgO (c), 1%-Pd/MgO (d), 2%-Pd/MgO (e), and 0.5%-Pd/MgO after 120 h of lifetime evaluation (f). The insets correspond to the size distributions of Pd nanoparticles supported on MgO.

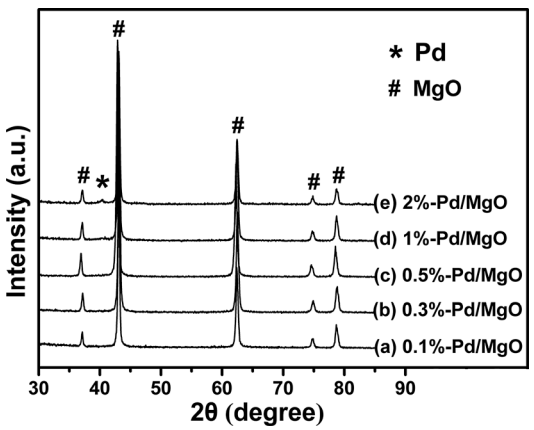

Fig. 4 XRD patterns of Pd/MgO catalysts with different Pd loadings.

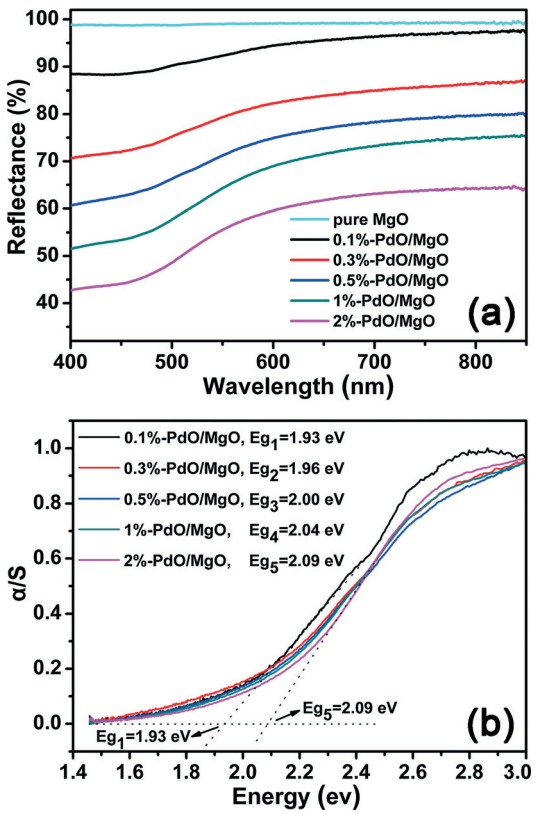

Fig. 5 (a) UV-DRS profiles of the pure MgO support and the calcined samples (PdO/MgO). (b) Tauc plots constructed from (a) according to the Kubelka–Munk function $\alpha/S = (1-R)^2/2R$; the ordinate values (α/S) have been normalized.

UV-DRS investigations were carried out for the characterization of the PdO species. Fig. 5a presents the UV-DRS profiles of the pure MgO support and the calcined PdO/MgO samples with various PdO loadings. For the pure MgO support, there are no absorption bands observable above 400 nm, while for PdO/MgO, there is only one broad absorption band with a maximum at about 620 nm, which can be assigned to the optical absorption edge of PdO.[23] The Kubelka–Munk function ($\alpha/S = (1-R)^2/2R$) is often used to evaluate the band gap of a semiconductor material in terms of the Tauc plot,[24] which is constructed by plotting the Kubelka–Munk function. The determined band gap of the PdO increases with the

increase of PdO loading (Fig. 5b), indicating a blue shift of the absorption edge. There is a significant difference (0.16 eV) between the band gaps of 0.1%-PdO/MgO and 2%-PdO/MgO. The UV-DRS results suggest that the coordination environment of the palladium species was changed due to the interaction between PdO and the MgO support, which was significantly affected by the PdO loading.

The results of the TPR experiments for the calcined samples (PdO/MgO) are presented in Fig. 6. A single peak was observed for all of the calcined samples and the intensity increased gradually along with the increase of the PdO loading. This reveals that the PdO species are reduced to metallic Pd and the amounts of H_2 consumed are closely associated with the PdO loading. Moreover, it should be noted that the reduction peak position of the maxima shifts towards higher temperatures from 73–93 °C as the PdO loading increases. This shift can be interpreted as the result of the enhancement of the interaction between PdO species and the MgO support, based on the characterization of UV-DRS. The strong interaction between PdO species and the MgO support can effectively prevent the aggregation and sintering of Pd nanoparticles during the hydrogen reduction process at high temperature, which can be verified by the TEM images (Fig. 3).

Fig. 7 displays the TPD profiles of CO_2 adsorbed on the pure MgO support and Pd/MgO catalysts with different Pd loadings. Several CO_2 desorption peaks are observed for all samples which can be classified into three types of basic sites with different strengths, *i.e.*, "weak" (CO_2 desorption between 27 and 147 °C), "medium" (CO_2 desorption between 147 and 377 °C), and "strong" (CO_2 desorption above 377 °C) basicity.[25] The "weak" basic sites are probably associated with Brønsted basicity and most likely originate from the lattice-bound OH groups. The "medium" and "strong" sites are probably correlated to Lewis basicity originating from the three- and four-fold-coordinated O^{2-} anions.[25] The CO_2-TPD profiles of Pd/MgO catalysts are similar to that of the pure MgO support, indicating that the surface basicity sites of the MgO support remained unchanged during the preparation of catalysts. A similar phenomenon was also observed by Shen *et al.*[26]

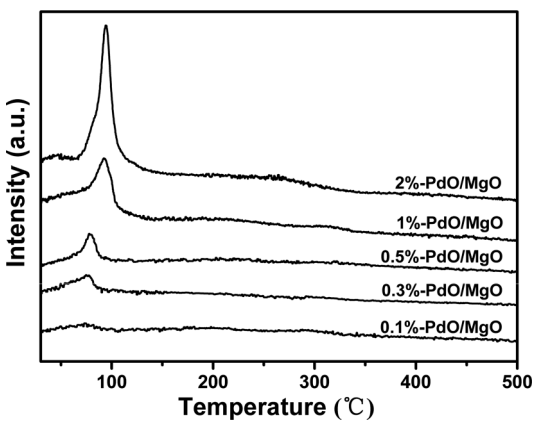

Fig. 6 H_2-TPR profiles of the calcined samples (PdO/MgO).

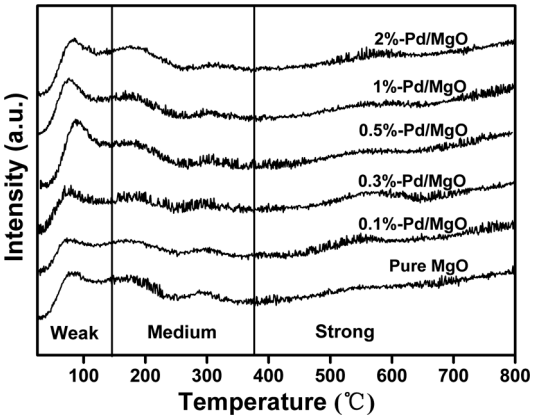

Fig. 7 CO_2-TPD profiles of the pure MgO support and Pd/MgO catalysts with different Pd loadings.

4. Conclusions

In summary, we firstly found that basic MgO can serve as an excellent support for Pd catalysts for CO oxidative coupling to DMO. The amount of Pd loading significantly affects the catalytic performance for CO oxidative coupling to DMO. The activity of the Pd/MgO catalyst increases with the increase of the Pd loading because of the high dispersion and similar sizes of the Pd nanoparticles, as well as the increase in number of surface active sites. The low Pd loading (*ca.* 0.5%) Pd/MgO catalyst exhibits excellent activity, selectivity and stability with 63% CO conversion and 97% selectivity to DMO after more than 120 h on stream at 130 °C. This work provides insight into designing high-performance catalysts for CO oxidative coupling to DMO by choosing appropriate supports. Further experimental and theoretical studies are still required to gain more insight into the origin of the role of the supports.

Acknowledgements

We gratefully acknowledge financial support from the 973 Program (2011CBA00505, 2013CB933200), the NSF of China (21003126, 21203200, 21303202), and the NSF of Fujian Province (2013J05034).

Notes and references

1 T.-J. Zhao, D. Chen, Y.-C. Dai, W.-K. Yuan and A. Holmen, *Ind. Eng. Chem. Res.*, 2004, **43**, 4595–4601.
2 Y.-N. Wang, X. P. Duan, J. W. Zheng, H. Q. Lin, Y. Z. Yuan, H. Ariga, S. Takakusagi and K. Asakura, *Catal. Sci. Technol.*, 2012, **2**, 1637–1639.
3 A.-Y. Yin, X.-Y. Guo, W.-L. Dai and K.-N. Fan, *Chem. Commun.*, 2010, **46**, 4348–4350.
4 Z. He, H. Q. Lin, P. He and Y. Z. Yuan, *J. Catal.*, 2011, **277**, 54–63.
5 J. D. Lin, X. Q. Zhao, Y. H. Cui, H. B. Zhang and D. W. Liao, *Chem. Commun.*, 2012, **48**, 1177–1179.

6 H. R. Yue, Y. J. Zhao, X. B. Ma and J. L. Gong, *Chem. Soc. Rev.*, 2012, **41**, 4218–4244.
7 L. Lin, P. B. Pan, Z. F. Zhou, Z. J. Li, J. X. Yang, M. L. Sun and Y. G. Yao, *Cuihua Xuebao*, 2011, **32**, 957–969.
8 Z. F. Zhou, Z. J. Li, P. B. Pan, L. Lin, Y. Y. Qin and Y. G. Yao, *Huagong Jinzhan*, 2010, **29**, 2003–2009.
9 D. M. Fenton and P. J. Steinwand, *J. Org. Chem.*, 1974, **39**, 701–704.
10 Q. Lin, Y. Ji, Z. D. Jiang and W. D. Xiao, *Ind. Eng. Chem. Res.*, 2007, **46**, 7950–7954.
11 X. G. Zhao, Q. Lin and W. D. Xiao, *Appl. Catal., A*, 2005, **284**, 253–257.
12 Y. Ji, G. Liu, W. Li and W. D. Xiao, *J. Mol. Catal. A: Chem.*, 2009, **314**, 63–70.
13 Z.-N. Xu, J. Sun, C.-S. Lin, X.-M. Jiang, Q.-S. Chen, S.-Y. Peng, M.-S. Wang and G.-C. Guo, *ACS Catal.*, 2013, **3**, 118–122.
14 S.-Y. Peng, Z.-N. Xu, Q.-S. Chen, Y.-M. Chen, J. Sun, Z.-Q. Wang, M.-S. Wang and G.-C. Guo, *Chem. Commun.*, 2013, **49**, 5718–5720.
15 S. Uchiumi, K. Ataka and T. Matsuzaki, *J. Organomet. Chem.*, 1999, **576**, 279–289.
16 D. Widmann, Y. Liu, F. Schuth and R. J. Behm, *J. Catal.*, 2010, **276**, 292–305.
17 M. Comotti, W.-C. Li, B. Spliethoff and F. Schuth, *J. Am. Chem. Soc.*, 2006, **128**, 917–924.
18 H. Yoshida, T. Nakajima, Y. Yazawa and T. Hattori, *Appl. Catal., B*, 2007, **71**, 70–79.
19 P. Sangeetha, K. Shanthi, K. S. R. Rao, B. Viswanathan and P. Selvam, *Appl. Catal., A*, 2009, **353**, 160–165.
20 S. Rojluechai, S. Chavadej, J. W. Schwank and V. Meeyoo, *Catal. Commun.*, 2007, **8**, 57–64.
21 T. Nanba, S. M. Asukawa, J. Uchisawa and A. Obuchi, *J. Catal.*, 2008, **259**, 250–259.
22 R. K. Marella, C. K. P. Neeli, S. R. R. Kamaraju and D. R. Burri, *Catal. Sci. Technol.*, 2012, **2**, 1833–1838.
23 C.-J. Huang, F.-M. Pan, H.-Y. Chen and L. Chang, *J. Appl. Phys.*, 2010, **108**, 053105.
24 J. Tauc, R. Grigorovici and A. Vancu, *Phys. Status Solidi*, 1966, **15**, 627–637.
25 Z. Liu, J. A. Cortes-Concepcion, M. Mustian and M. D. Amiridis, *Appl. Catal., A*, 2006, **302**, 232–236.
26 S. Li, C. H. Chen, E. S. Zhan, S.-B. Liu and W. J. Shen, *J. Mol. Catal. A: Chem.*, 2009, **304**, 88–94.

